

Single-Particle Cryo-EM at Crystallographic Resolution

Yifan Cheng^{1,*}

¹Department of Biochemistry and Biophysics, University of California San Francisco, 600 16th Street, San Francisco, CA 94158, USA

*Correspondence: ycheng@ucsf.edu

<http://dx.doi.org/10.1016/j.cell.2015.03.049>

Until only a few years ago, single-particle electron cryo-microscopy (cryo-EM) was usually not the first choice for many structural biologists due to its limited resolution in the range of nanometer to subnanometer. Now, this method rivals X-ray crystallography in terms of resolution and can be used to determine atomic structures of macromolecules that are either refractory to crystallization or difficult to crystallize in specific functional states. In this review, I discuss the recent breakthroughs in both hardware and software that transformed cryo-microscopy, enabling understanding of complex biomolecules and their functions at atomic level.

A major goal of structural biology is to provide mechanistic understanding of critical biological processes. The most detailed insights come from atomic structures of macromolecules and complexes involved in these processes in relevant functional states. Beyond basic research, obtaining atomic structures of drug targets is also a standard approach in the pharmaceutical industry in the design and optimization of therapeutic compounds.

Prior to 2013, most atomic structures deposited in the protein data bank (PDB) were determined by X-ray crystallography. This technique starts with crystallization of molecules that are homogeneous in both composition and conformation. Once the 3D crystals are of sufficient size to diffract X-rays, they are used for structure determination. The resolution of crystal structures is largely determined by how well the molecules are ordered (or aligned to each other) in the crystal. After 100 years of development and maturation, X-ray crystallography has become a routine method, delivering a wealth of structural information about important biomolecules and cellular processes (Jones, 2014; Shi, 2014). While X-ray crystallography will continue to play an important role in answering many biological questions, it completely depends on growth of well-ordered 3D crystals. Producing such crystals, however, is a major bottleneck for challenging targets, such as integral membrane proteins of mammalian origin or chromatin in complex with its modifiers. In the last 2 years, single particle electron cryo-microscopy (cryo-EM) has emerged as a technique for determining atomic resolution structures at better than 4-Å resolution, comparable to many solved using crystallographic approaches. It has now determined a number of structures of proteins and complexes that have vexed crystallographers.

The Way Electron Cryo-Microscopy Works

Rather than determining structures from diffraction of 3D crystals, single-particle cryo-EM determines structures by computationally combining images of many individual macromolecules in identical or similar conformations (Frank et al., 1978). In this

approach, samples of purified molecules in solution are applied to an EM grid covered with a thin holey carbon film and blotted by a filter paper to remove most of solution so that a thin liquid layer is formed across the holes in the carbon film. This is followed by plunge-freezing in liquid ethane cooled by liquid nitrogen. This method was originally developed by Dubochet and colleagues (Dubochet et al., 1982), and improved significantly with semi-automated plunge-freezer machine to improve reproducibility. After plunge-freezing, frozen-hydrated molecules are embedded in a thin layer of vitreous ice (Figure 1A) that preserves the native structure to the atomic level (Taylor and Glaeser, 1974), prevents dehydration of biological samples within the vacuum of an electron microscope, and reduces the effects of radiation damage (Stark et al., 1996). Molecules embedded in a thin layer of vitreous ice adopt a range of orientations, which are then imaged using an electron beam (Figure 1B). Each particle image is a 2D projection of a molecule, whose spatial orientation and position are defined by six geometric parameters. These include three Euler angles and two in-plane positional parameters. The sixth parameter is the defocus that defines the z position along the direction of the electron beam and is often assumed to be the same for all particles in a micrograph (or image). After further correction for aberrational errors of the microscope, a 3D structure can be reconstructed by combining images of many molecules that have been aligned to each other. The resolution of the reconstruction is improved iteratively by refining the first five geometric parameters for each particle to high accuracy (Frank, 1996). The final 3D reconstruction is a Coulomb potential density map that can be interpreted in the same way as electron density maps determined by X-ray crystallography (Figures 1C and 1D).

Both X-ray and electron beams cause radiation damage to biological samples. For X-ray diffraction, a larger crystal with coherently packed molecules can tolerate a high total dose and often diffracts to high resolution because more molecules contribute to the diffraction. For single-particle cryo-EM, the total electron dose used to image each molecule is set to a very low

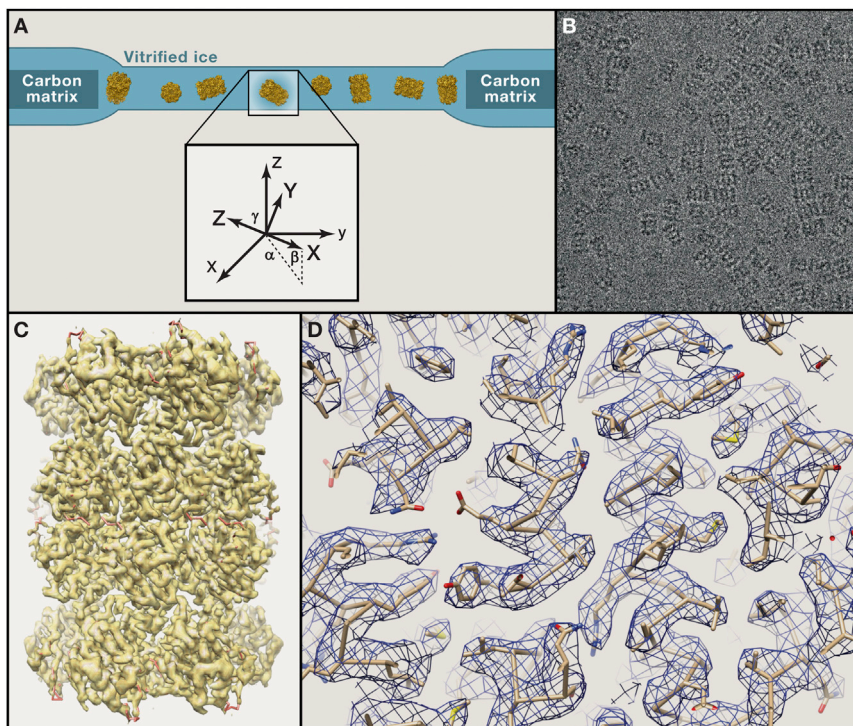


Figure 1. Single-Particle Cryo-EM

(A) Purified biological molecules are embedded in a thin layer of vitreous ice, in which they ideally adopt random orientations. The orientations are specified by the in-plane position parameters, x and y , and three Euler angles α , β , and γ , which are refined iteratively to high accuracies. The defocus values of the images are currently often determined separately.

(B) Typical image of frozen-hydrated archaeal 20S proteasomes.

(C) 3D reconstruction of the 20S proteasome at 3.3-Å resolution.

(D) Side-chain densities of the map shown in (B) are comparable with those seen in maps determined by X-ray crystallography at a similar resolution.

level to preserve structural information at the subnanometer-resolution level. The consequence of such low-dose imaging is that individual images have a very poor signal-to-noise ratio (SNR). Hence, images from many identical or similar molecules must be averaged to enhance the SNR as well as to provide the different views needed to calculate a 3D reconstruction (De Rosier and Klug, 1968). Therefore, the total number of particle images used in a reconstruction has a similar significance to the size of a 3D crystal. Similarly, the accuracy of image alignment in single-particle EM is analogous to how well molecules are packed in a 3D crystal.

Provided that a sufficient number of images containing high-resolution information are classified and aligned accurately, single-particle cryo-EM will produce a 3D reconstruction at atomic resolution. An atomic model can then be built de novo based on fitting the known sequences into the density map from the reconstruction. Furthermore, electron micrographs are real-space images containing both amplitude and phase information. Thus, cryo-EM structure determination does not have a “phase problem” as in X-ray crystallography, but its amplitudes are less accurate than that measured from X-ray diffractions.

Resolution Determinants of Single-Particle Cryo-EM Reconstructions

Considering the scattering power of electrons versus X-rays, and the amount of information present in an image of a single molecule that can be used to determine the precise position and orientation of the molecule, Richard Henderson predicted that single-particle cryo-EM can, in theory, determine atomic-resolution structures of biological molecules as small as 100 kDa in molecular weight (Henderson, 1995). However, there are many

obstacles took many years, but by 2008, it was possible to achieve resolutions that were sufficient to visualize side-chain densities (~ 3.8 Å) (Yu et al., 2008; Zhang et al., 2008), and to determine the first de novo atomic structure (3.3 Å) of a non-enveloped icosahedral virus (Zhang et al., 2010). Because of their large sizes and high symmetry, icosahedral virus particles were among the first for which high-resolution maps were obtained, and now it is quite feasible to determine reconstructions of such samples at resolutions better than 4 Å (Chen et al., 2009; Wolf et al., 2010; Yu et al., 2011). However, it has been much harder to achieve similar resolutions for molecules that are smaller and/or less symmetric.

Nowadays, an electron microscope with 200 kV or 300 kV acceleration voltage and a field emission gun (FEG) electron source can typically deliver images with a resolution of better than 2 Å. Therefore, the achievable resolution of single particle cryo-EM is not limited by the resolution power of a modern microscope itself, but rather by the conditions required to image frozen-hydrated biological samples and the unique properties of such samples. Determining a high-resolution 3D reconstruction requires that 2D projection images contain sufficient information at both high and low resolutions. The amount of high-resolution information present in images determines the possible final resolution of a 3D reconstruction. However, low-resolution information, i.e., image contrast, is also required to visualize particles. Together, they determine how well a homogeneous set of molecules can be computationally selected for averaging, how accurately these images can be aligned, and the total number of images that are required to achieve a certain resolution. For any electron micrographs, both image amplitudes and phases are modulated by the contrast transfer function (CTF) of the

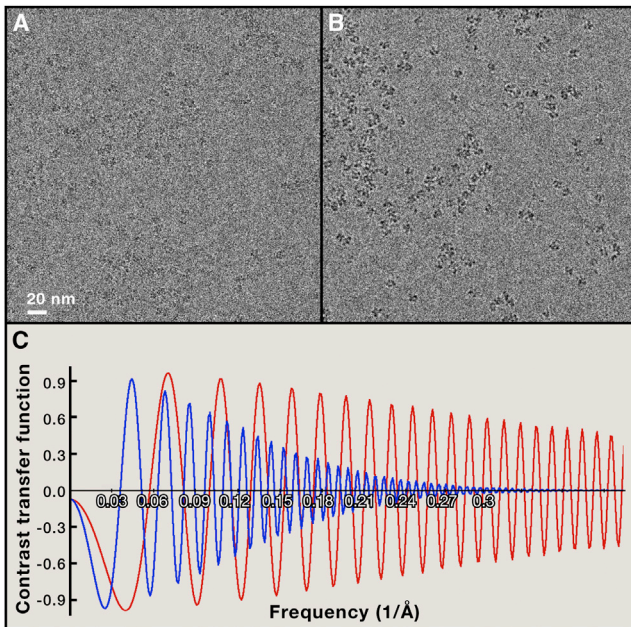


Figure 2. Influence of CTF on Image Contrast and Resolution

(A and B) Image of human transferrin receptor-transferrin complex recorded using a scintillator camera. The microscope was equipped with a FEG and operated at 200 kV. Particles in image recorded with a defocus of 1.2 μm (A) are almost invisible, but shown with strong contrast in the image recorded with a defocus of 3.0 μm (B).

(C) Simulations of CTF at 1.2 μm (red) and 3.0 μm (blue) defoci, with an acceleration voltage of 200 kV and angular spread of 0.07 mrad. Note that 3 μm defocus generates sufficient contrast for particles with a molecular weight of ~ 300 kDa, CTF envelope drops to close to zero at 3- ~ 4 - \AA resolution.

microscope, which is mostly a sine function with an envelope that reduces the amplitude at high resolution, such as shown in Figure 2C. The overall envelope of the CTF function combines effects from many factors, including the spatial and temporal coherence of the electron beam, specimen motion, the modulation transfer function (MTF) of the image recording device, and others. The contribution of the spatial coherence to the envelope is also a function of the defocus. A small defocus maximizes the envelope at high resolution but minimizes the CTF at low resolution. Thus, to obtain the best high-resolution signal, an image must be recorded with a small defocus, which results, however, in a poor image contrast. The converse is also true: to obtain good contrast, an image has to be recorded with a relatively large defocus, which reduces, however, the high-resolution signal (Figure 2). Both low- and high-resolution signals are further reduced by the MTF of the image-recording device.

This is not a serious problem for a radiation-resistant specimen. Using a sufficient electron dose, a modern electron microscope can image, for example, a single layer of graphene at atomic or near-atomic resolution with good contrast (Urban, 2011). The weak low-resolution signal is compensated by a high-electron dose, which generates sufficient image contrast. However, this approach is not possible for biological samples, which are sensitive to radiation damage (Henderson and Glaeser, 1985). To visualize frozen-hydrated biological mole-

cules with sufficient contrast, one has to record images with some defocus (Figures 2A and 2B), which causes a reduction in the high-resolution signal (Figure 2C). Hence, imaging frozen-hydrated biological molecules always requires a fine balance between contrast and resolution. Note that such balance is always influenced by the microscope hardware, such as the spatial coherence of the electron beam, the image recording device, etc., as well as by the size and symmetry of the molecule being studied.

The first breakthrough in boosting the resolution of single-particle cryo-EM maps came from the use of FEGs, which generate an electron beam with much better spatial coherence than a thermo-ionic electron source (Zhou and Chiu, 1993). While FEGs do not change the oscillation of the CTF function, at the same defocus, high-resolution signal is better preserved in images recorded with a microscope equipped with a FEG than with a thermo-ionic electron source. FEGs thus enable structure determinations at subnanometer resolutions for molecules ranging from icosahedral viruses (Böttcher et al., 1997; Conway et al., 1997; Zhou et al., 2000) to molecules as small as ~ 300 kDa with mere 2-fold symmetry (Cheng et al., 2004).

Manufacturers made many efforts to improve microscope performance. State-of-the-art electron microscopes nowadays use constant-power electromagnetic lenses to improve stability, parallel illumination to reduce image phase error induced by beam tilt (Glaeser et al., 2011), very high vacuum to reduce water contamination on frozen-hydrated samples loaded into the microscope column, and better computer control for sophisticated and automated microscope tuning and data acquisition (Suloway et al., 2005), etc. All these features helped to improve the efficiency of as well as the resolution achievable by single-particle cryo-EM, and they eventually enabled the first de novo atomic structure determination of an icosahedral virus (Zhang et al., 2010). Large and highly symmetrical particles, such as icosahedral viruses, have certain advantages in achieving better resolution by single-particle cryo-EM. They can be imaged with very small defocus to preserve the high-resolution signal while still provide sufficient image contrast. However, the same approach does not work for small molecules. Images of small molecules must be recorded using a much larger defocus, thus trading high-resolution signal for image contrast. The need to use a relatively large defocus to generate image contrast was a major obstacle in achieving even subnanometer-resolution maps for proteins smaller than 300 kDa without high symmetry. Overcoming these limitations required new technologies. The simple use of small defocus without any other means to generate sufficient image contrast led to featureless images and controversial results (Henderson, 2013; Mao et al., 2013).

Recent Technological Advances in Single-Particle Cryo-EM

Some recent technological advances led to a major breakthrough in achievable resolution, resulting, in a short period of time, in 3- to ~ 5 - \AA -resolution structures of biological molecules ranging from ribosomal particles to integral membrane proteins (Allegretti et al., 2014; Amunts et al., 2014; Liao et al., 2013; Lu et al., 2014; Vinothkumar et al., 2014). Some of these structures were determined for proteins with known atomic structures,

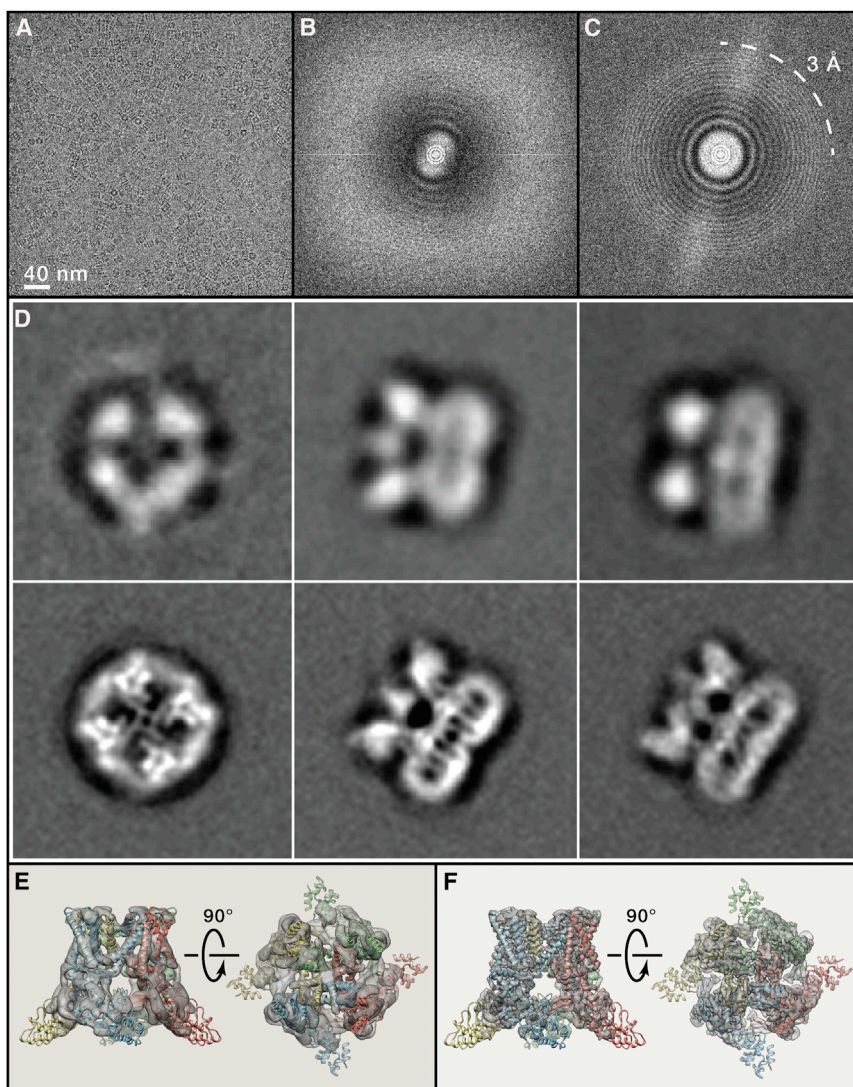


Figure 3. Direct Electron Detection Camera Enabled Major Breakthroughs in Single Particle Cryo-EM

(A) An image of frozen hydrated *T. acidophilum* 20S proteasome recorded using K2 Summit camera with a 300-kV microscope and a defocus of $\sim 0.9 \mu\text{m}$.

(B) Fourier transform of a typical imperfect image of frozen hydrated 20S proteasome, showing a predominant resolution cutoff caused by beam-induced motion.

(C) Fourier transform of the same image after motion correction. Thin ring is restored to resolution of $\sim 3 \text{ \AA}$.

(D) 2D class averages of TRPV1 ion channel calculated from images recorded with a scintillator camera (left) and K2 Summit camera (right) (Liao et al., 2013).

(E) Two different views of TRPV1 3D reconstruction determined from a dataset collected with a scintillator camera.

(F) Same views of the TRPV1 3D reconstruction determined from a dataset collected with a K2 Summit camera. (A–C) are reproduced from (Li et al., 2013).

spatial frequency, leading to poor image contrast. Thus, recording on photographic film typically requires imaging at a higher defocus to ensure sufficient contrast for reliable particle picking and accurate image alignment. Scintillator-based cameras have a better low-frequency DQE than photographic film, resulting in a better image contrast. However, the high-frequency DQE of these cameras is significantly poorer than that of film, making them less suitable for high-resolution imaging (Booth et al., 2006; Meyer et al., 2000).

As their name suggests, the new direct electron detection cameras no longer convert electron signals to light signals

but detect the electrons directly (McMullan et al., 2009b; McMullan et al., 2009c). All commercially available direct detection cameras have significantly higher DQEs than photographic film and scintillator-based cameras in both the low- and high-resolution regimes (Li et al., 2013; McMullan et al., 2014; Ruskin et al., 2013). These cameras typically operate in two distinct modes, the linear charge-integration mode or the electron-counting mode. In the linear mode, charges generated from electrons striking the detector are integrated, while in the counting mode individual electron events are identified and counted. An advantage of operating in the counting mode is that both Landau noise (i.e., the fluctuation in energies generated by each electron striking the camera sensor) and readout noise are removed. Combining direct electron detection with single electron counting significantly improves the DQE further, particularly at low frequencies (Li et al., 2013). Electron-counting cameras thus enable recording low-dose cryo-EM images of small particles with much smaller defocus values (Figure 3A), providing a much

Camera Technology

validating the methodological advancements (Bartesaghi et al., 2014; Li et al., 2013). Others were determined ab initio for proteins that resisted crystallization for years (Liao et al., 2013; Lu et al., 2014). Here, I will briefly summarize the recent technological advancements and how they enabled a “resolution revolution” (Kühlbrandt, 2014).

Image-recording devices are characterized by the detective quantum efficiency (DQE), which describes the signal and noise performance in a digitally recorded image over the spatial frequency range (McMullan et al., 2009a; Mooney, 2007). Traditionally, EM images were recorded on photographic film that was subsequently digitized or with scintillator-based digital cameras, such as charge-coupled device (CCD) or complementary metal-oxide semiconductor (CMOS) cameras. These cameras use a thin layer of phosphor scintillator to convert electron signals to photons, which are coupled through fiber optics to the camera sensor. Photographic film has a relative poor DQE at low

but detect the electrons directly (McMullan et al., 2009b; McMullan et al., 2009c). All commercially available direct detection cameras have significantly higher DQEs than photographic film and scintillator-based cameras in both the low- and high-resolution regimes (Li et al., 2013; McMullan et al., 2014; Ruskin et al., 2013). These cameras typically operate in two distinct modes, the linear charge-integration mode or the electron-counting mode. In the linear mode, charges generated from electrons striking the detector are integrated, while in the counting mode individual electron events are identified and counted. An advantage of operating in the counting mode is that both Landau noise (i.e., the fluctuation in energies generated by each electron striking the camera sensor) and readout noise are removed. Combining direct electron detection with single electron counting significantly improves the DQE further, particularly at low frequencies (Li et al., 2013). Electron-counting cameras thus enable recording low-dose cryo-EM images of small particles with much smaller defocus values (Figure 3A), providing a much

better balance between the requirements for both image contrast and high-resolution signal (Li et al., 2013; Liao et al., 2013; Lu et al., 2014).

Another important feature of the newly developed direct detection cameras is their fast frame readout rate. It enables the already low total electron dose used to image biological samples to be fractionated into many subframes. Computational alignment of these subframes before averaging them can correct for motion-induced image blurring, which results from beam-induced image motion and mechanical instability of the specimen holder (Bai et al., 2013; Brilot et al., 2012; Campbell et al., 2012; Li et al., 2013). The combination of dose fractionation and motion correction greatly improves the efficiency of data acquisition, because nearly all images can be corrected to recover high-resolution information (Figures 3B and 3C). It also provides novel means to optimize usage of the total electron dose (Baker and Rubinstein, 2010). The contrast can be maximized by using a higher total dose and using all frames for particle alignment. However, the later frames that record images of molecules with higher accumulated electron dose and thus more severe radiation damage can later be eliminated or properly down-weighted so as to minimize the effect of radiation damage on the final 3D reconstruction (Li et al., 2013; Scheres, 2014). These novel technologies are now being applied in many cryo-EM laboratories. They marked the beginning of a new era in single-particle cryo-EM, in which atomic structures of a broad range of biological macromolecules can be determined de novo and without crystallization (Figures 3D–3F).

Maximum Likelihood-Based Classification

A major advantage of single-particle cryo-EM is that it does not require absolute sample homogeneity. Computational image analysis can deal with a certain level of heterogeneity, both conformational and compositional. Such heterogeneity may prevent crystallization, but in single-particle EM, particles can be computationally sorted into different classes, some of which may contain relatively homogeneous subsets of particles. Single-particle cryo-EM datasets consist of 2D projection images. As determining the orientation parameters of these 2D projections is intertwined with the classification of a heterogeneous dataset into homogeneous subsets, it is always challenging to distinguish whether different 2D projection images represent different views of the same molecule or views of molecules with different conformations or compositions. While there are many ways to classify particles according to their conformations or functional states, a particularly powerful approach is to use a maximum likelihood-based method for classification and refinement (Scheres et al., 2007). Implementing sophisticated maximum likelihood-based classification and refinement algorithms (Sigworth, 1998; Sigworth et al., 2010) into user-friendly software packages (Lyumkis et al., 2013; Scheres, 2010, 2012) made this method easy to use in practice. It has become routine now to classify particle images into different 3D classes, each of which may be amenable to refinement into higher-resolution reconstructions than the global ensemble. The process of 3D classification may separate a number of conformations of the molecule being studied, or separate fully intact particles or complexes from incomplete, truncated or fragmented complexes, or from those damaged during vitrification (Fernández et al., 2013;

Liao et al., 2014). Note that the better image quality provided by direct detection cameras and motion correction enabled success of these classification procedures. Almost all newly published near-atomic resolution 3D reconstructions, in one way or another, utilized such classification procedures.

The use of automated data acquisition (Suloway et al., 2005) with automated particle-picking procedures enables collecting very large datasets with millions of particle images in relatively short periods of time. With large numbers of particles it will be possible to classify particle images with very subtle conformational differences and thus to detect and quantify even subtle conformational states that exist within a population. This has been achieved at somehow moderate resolution (Fischer et al., 2010). It is only a matter of resources and time before single-particle cryo-EM is able to provide solution structures of molecules in multiple conformations at near-atomic resolution and to provide quantitative comparisons of population occupancies under different conditions.

Single-Particle Cryo-EM Is Complementary to X-Ray Crystallography

There are many large protein assemblies and dynamic complexes that are difficult or may even be impossible to crystallize. Thus, single-particle cryo-EM has always been viewed as a supplementary method to X-ray crystallography for studying such assemblies or complexes, such as clathrin coats (Fotin et al., 2004), the 26S proteasome (da Fonseca et al., 2012; Lander et al., 2012; Lasker et al., 2012), the anaphase promoting complex (Chang et al., 2014; da Fonseca et al., 2011), and chromatin fibers (Song et al., 2014), to name just a few. In these studies, structures were typically determined by single-particle methods to subnanometer resolution. Crystal structures of domains and fragments or sequence-based homology models were then fitted into the cryo-EM density maps by molecular dynamic simulations or other computational methods (DiMaio et al., 2015; Seidelt et al., 2009; Trabuco et al., 2009; Zhao et al., 2013). Such hybrid approaches made, for example, subnanometer-resolution structures of integral membrane proteins very meaningful in providing rich structural insights into large membrane protein complexes (Efremov et al., 2015; Vinothkumar et al., 2014) or for dissecting function-related conformational changes (Kim et al., 2014; Meyerson et al., 2014).

With the resolution improved to a level sufficient for sequence-based de novo model building, structures determined by single-particle cryo-EM are comparable to those determined from crystals (Bartesaghi et al., 2014; Li et al., 2013). Therefore, for many difficult crystallographic targets, either because they are refractory to crystallization or difficult to express and purify in sufficient quantities for crystallization, single-particle cryo-EM is becoming the *method-of-choice* for structure determination. Recent successes in structure determination of mammalian integral membrane proteins clearly demonstrated this capability (Liao et al., 2013; Lu et al., 2014; Yan et al., 2015; Zalk et al., 2015). Even for those targets that could be crystallized, it is now feasible to use single-particle cryo-EM to determine high-resolution structures of the targets in specific functional states or in complexes with co-factors. We can anticipate that such successes will continue rapidly, with many more structures of

various types of biological molecules being determined to near-atomic resolution. Besides large complexes such as ribosome and icosahedral viruses, integral membrane proteins or membrane protein complexes will be a major area in which single-particle cryo-EM will play a role that is equally significant as X-ray crystallography. Another class of targets that is difficult to crystallize but suitable for single-particle cryo-EM is chromatin in complex with its modifiers, which is essential for understanding the complexities of gene expression. Progress of crystallographic studies in this area has been slow with only a few atomic structures available for nucleosomes alone or in complex with modifiers, each having led to major discoveries in chromatin biology (Cramer, 2014). Recent work, although still limited to nanometer resolution, has shown the tremendous promise of single-particle cryo-EM in this important structural biology field (Song et al., 2014).

Future Perspectives for Single-Particle Cryo-EM

Without a doubt, single-particle cryo-EM is no longer “blobology” but is now a method that can provide resolutions comparable with X-ray crystallography. However, unlike X-ray crystallography, which often ends up with a binary result of either having or not having a diffracting crystal, single-particle cryo-EM always yields some information (although not always at atomic resolution). Even a reconstruction at a modest resolution provides information of how to improve the preparation as well as valuable biological insights. Thus, single-particle cryo-EM is probably even more attractive than X-ray crystallography in studying macromolecules.

However, the technology of single-particle cryo-EM is still far from perfect and technological developments are still moving forward rapidly. The current resolution is still unsatisfactory in many ways. For example, extending the achievable resolution to beyond 3 Å is necessary to convincingly visualize the location of ions, or to visualize not only where but also how small ligand molecules bind to target proteins. The latter is of particular interest for the pharmaceutical industry because it can facilitate structure-based drug design and optimization. A recent review discusses in detail the current technical limitations of single-particle cryo-EM, particularly in achieving higher resolution, and possible solutions (Agard et al., 2014). Related to insufficient resolution, time spent on de novo model building and refinement is often far more than that used to determine the reconstruction itself. While many tools from X-ray crystallography can be applied to cryo-EM density map-based model building and refinement, it requires significant modifications (Amunts et al., 2014; Brown et al., 2015). Also, the traditional validation criterion in X-ray crystallography, such as the free R-factor, is no longer valid for models built into cryo-EM density maps. Therefore, tools and methodologies for efficient model building, refinement, and validation all need further developments.

In addition to improving the technology itself, there are other factors that limit the wide application of single-particle cryo-EM. First, the method itself is not yet a “turnkey” method. Even with automated data acquisition technology and streamlined data processing, image acquisition, and processing is still too complex for a novice to learn with minimal training or by studying manuals. Second, the needed infrastructure, including

fully functional cryo-EM equipment and computational resources for data processing and storage, requires significant financial investment. In addition to the initial investment, the ongoing costs required to maintain and operate a high-end cryo-EM facility are significant. Third, there are currently too few synchrotron-like cryo-EM facilities dedicated for high-throughput cryo-EM data acquisition for the community at large. These limitations set the threshold for entering the field far too high, and improving access will require efforts from multiple parties. Therefore, making the technology robust and relatively easy to learn, reducing the equipment and operational costs, and providing access to ready-to-use facilities staffed with experts will all be important steps toward making cryo-EM as widely used as X-ray crystallography. While the future of single-particle cryo-EM is bright, it requires strong support from the scientific community as well as from funding agencies to make the single particle cryo-EM as popular as X-ray crystallography.

ACKNOWLEDGMENTS

I thank T. Walz, T. Gonen, A. Frost, and members of my laboratory for critical reading of the manuscript. Cryo-EM work in the Cheng laboratory is supported by grants from the NIH (R01GM098672, R01GM082893 and S10RR026814 to Y.C. and P50GM082250 to A. Frankel), the NSF (DBI-0960271 to D.A.A and Y.C.), which in part funded the development of the K2 camera in association with Gatan and P. Denes at Lawrence Berkeley Laboratory, and the University of California San Francisco Program for Breakthrough Biomedical Research (to Y.C.). Note that the goal of this review is to introduce single-particle cryo-EM to a broad audience by comparing it with the well-established method of X-ray crystallography; it is not meant to be a comprehensive review of single-particle cryo-EM, nor of the history of its methodological developments. I apologize to the many colleagues whose important contributions I was unable to cite due to space limitations.

REFERENCES

- Agard, D.A., Cheng, Y., Glaeser, R.M., and Subramaniam, S. (2014). Chapter Two – Single-particle cryo-electron microscopy (cryo-EM): progress, challenges, and perspectives for future improvement. *Adv. Imaging Electron Phys.* 185, 113–137.
- Allegretti, M., Mills, D.J., McMullan, G., Kühlbrandt, W., and Vonck, J. (2014). Atomic model of the F420-reducing [NiFe] hydrogenase by electron cryo-microscopy using a direct electron detector. *eLife* 3, e01963.
- Amunts, A., Brown, A., Bai, X.C., Llácer, J.L., Hussain, T., Emsley, P., Long, F., Murshudov, G., Scheres, S.H., and Ramakrishnan, V. (2014). Structure of the yeast mitochondrial large ribosomal subunit. *Science* 343, 1485–1489.
- Bai, X.C., Fernandez, I.S., McMullan, G., and Scheres, S.H. (2013). Ribosome structures to near-atomic resolution from thirty thousand cryo-EM particles. *eLife* 2, e00461.
- Baker, L.A., and Rubinstein, J.L. (2010). Radiation damage in electron cryomicroscopy. *Methods Enzymol.* 481, 371–388.
- Bartesaghi, A., Matthies, D., Banerjee, S., Merk, A., and Subramaniam, S. (2014). Structure of β -galactosidase at 3.2-Å resolution obtained by cryo-electron microscopy. *Proc. Natl. Acad. Sci. USA* 111, 11709–11714.
- Booth, C.R., Jakana, J., and Chiu, W. (2006). Assessing the capabilities of a 4kx4k CCD camera for electron cryo-microscopy at 300kV. *J. Struct. Biol.* 156, 556–563.
- Böttcher, B., Wynne, S.A., and Crowther, R.A. (1997). Determination of the fold of the core protein of hepatitis B virus by electron cryomicroscopy. *Nature* 386, 88–91.

- Brilot, A.F., Chen, J.Z., Cheng, A., Pan, J., Harrison, S.C., Potter, C.S., Carragher, B., Henderson, R., and Grigorieff, N. (2012). Beam-induced motion of vitrified specimen on holey carbon film. *J. Struct. Biol.* *177*, 630–637.
- Brown, A., Long, F., Nicholls, R.A., Toots, J., Emsley, P., and Murshudov, G. (2015). Tools for macromolecular model building and refinement into electron cryo-microscopy reconstructions. *Acta Crystallogr. D Biol. Crystallogr.* *71*, 136–153.
- Campbell, M.G., Cheng, A., Brilot, A.F., Moeller, A., Lyumkis, D., Veessler, D., Pan, J., Harrison, S.C., Potter, C.S., Carragher, B., and Grigorieff, N. (2012). Movies of ice-embedded particles enhance resolution in electron cryo-microscopy. *Structure* *20*, 1823–1828.
- Chang, L., Zhang, Z., Yang, J., McLaughlin, S.H., and Barford, D. (2014). Molecular architecture and mechanism of the anaphase-promoting complex. *Nature* *513*, 388–393.
- Chen, J.Z., Settembre, E.C., Aoki, S.T., Zhang, X., Bellamy, A.R., Dormitzer, P.R., Harrison, S.C., and Grigorieff, N. (2009). Molecular interactions in rotavirus assembly and uncoating seen by high-resolution cryo-EM. *Proc. Natl. Acad. Sci. USA* *106*, 10644–10648.
- Cheng, Y., Zak, O., Aisen, P., Harrison, S.C., and Walz, T. (2004). Structure of the human transferrin receptor-transferrin complex. *Cell* *116*, 565–576.
- Conway, J.F., Cheng, N., Zlotnick, A., Wingfield, P.T., Stahl, S.J., and Steven, A.C. (1997). Visualization of a 4-helix bundle in the hepatitis B virus capsid by cryo-electron microscopy. *Nature* *386*, 91–94.
- Cramer, P. (2014). A tale of chromatin and transcription in 100 structures. *Cell* *159*, 985–994.
- da Fonseca, P.C., Kong, E.H., Zhang, Z., Schreiber, A., Williams, M.A., Morris, E.P., and Barford, D. (2011). Structures of APC/C(Cdh1) with substrates identify Cdh1 and Apc10 as the D-box co-receptor. *Nature* *470*, 274–278.
- da Fonseca, P.C., He, J., and Morris, E.P. (2012). Molecular model of the human 26S proteasome. *Mol. Cell* *46*, 54–66.
- De Rosier, D.J., and Klug, A. (1968). Reconstruction of three dimensional structures from electron micrographs. *Nature* *217*, 130–134.
- DiMaio, F., Song, Y., Li, X., Brunner, M.J., Xu, C., Conticello, V., Egelman, E., Marlovits, T.C., Cheng, Y., and Baker, D. (2015). Atomic-accuracy models from 4.5-Å cryo-electron microscopy data with density-guided iterative local refinement. *Nat. Methods* *12*, 361–365.
- Dubochet, J., Chang, J.J., Freeman, R., Lepault, J., and McDowell, A.W. (1982). Frozen aqueous suspensions. *Ultramicroscopy* *10*, 55–61.
- Efremov, R.G., Leitner, A., Aebersold, R., and Raunser, S. (2015). Architecture and conformational switch mechanism of the ryanodine receptor. *Nature* *517*, 39–43.
- Fernández, I.S., Bai, X.C., Hussain, T., Kelley, A.C., Lorsch, J.R., Ramakrishnan, V., and Scheres, S.H. (2013). Molecular architecture of a eukaryotic translational initiation complex. *Science* *342*, 1240585.
- Fischer, N., Konevega, A.L., Wintermeyer, W., Rodnina, M.V., and Stark, H. (2010). Ribosome dynamics and tRNA movement by time-resolved electron cryomicroscopy. *Nature* *466*, 329–333.
- Fotin, A., Cheng, Y., Sliz, P., Grigorieff, N., Harrison, S.C., Kirchhausen, T., and Walz, T. (2004). Molecular model for a complete clathrin lattice from electron cryomicroscopy. *Nature* *432*, 573–579.
- Frank, J. (1996). Three-dimensional electron microscopy of macromolecular assembly, 2 edn (Oxford University Press).
- Frank, J., Goldfarb, W., Eisenberg, D., and Baker, T.S. (1978). Reconstruction of glutamine synthetase using computer averaging. *Ultramicroscopy* *3*, 283–290.
- Glaeser, R.M., Typke, D., Tiemeijer, P.C., Pulokas, J., and Cheng, A. (2011). Precise beam-tilt alignment and collimation are required to minimize the phase error associated with coma in high-resolution cryo-EM. *J. Struct. Biol.* *174*, 1–10.
- Henderson, R. (1995). The potential and limitations of neutrons, electrons and X-rays for atomic resolution microscopy of unstained biological molecules. *Q. Rev. Biophys.* *28*, 171–193.
- Henderson, R. (2013). Avoiding the pitfalls of single particle cryo-electron microscopy: Einstein from noise. *Proc. Natl. Acad. Sci. USA* *110*, 18037–18041.
- Henderson, R., and Glaeser, R.M. (1985). Quantitative analysis of image contrast in electron micrographs of beam-sensitive crystals. *Ultramicroscopy* *16*, 139–150.
- Jones, N. (2014). Crystallography: Atomic secrets. *Nature* *505*, 602–603.
- Kim, J., Wu, S., Tomasiak, T., Mergel, C.M., Winter, M.B., Stiller, S.B., Robles-Colmanares, Y., Stroud, R.M., Tampe, R., Craik, C.S., et al. (2014). Subnanometre-resolution electron cryomicroscopy structure of a heterodimeric ABC exporter. *Nature* *517*, 396–400.
- Kühlbrandt, W. (2014). Biochemistry. The resolution revolution. *Science* *343*, 1443–1444.
- Lander, G.C., Estrin, E., Matyskiela, M.E., Bashore, C., Nogales, E., and Martin, A. (2012). Complete subunit architecture of the proteasome regulatory particle. *Nature* *482*, 186–191.
- Lasker, K., Förster, F., Bohn, S., Walzthoeni, T., Villa, E., Unverdorben, P., Beck, F., Aebersold, R., Sali, A., and Baumeister, W. (2012). Molecular architecture of the 26S proteasome holocomplex determined by an integrative approach. *Proc. Natl. Acad. Sci. USA* *109*, 1380–1387.
- Li, X., Mooney, P., Zheng, S., Booth, C.R., Braunfeld, M.B., Gubbens, S., Agard, D.A., and Cheng, Y. (2013). Electron counting and beam-induced motion correction enable near-atomic-resolution single-particle cryo-EM. *Nat. Methods* *10*, 584–590.
- Liao, M., Cao, E., Julius, D., and Cheng, Y. (2013). Structure of the TRPV1 ion channel determined by electron cryo-microscopy. *Nature* *504*, 107–112.
- Liao, M., Cao, E., Julius, D., and Cheng, Y. (2014). Single particle electron cryomicroscopy of a mammalian ion channel. *Curr. Opin. Struct. Biol.* *27*, 1–7.
- Lu, P., Bai, X.C., Ma, D., Xie, T., Yan, C., Sun, L., Yang, G., Zhao, Y., Zhou, R., Scheres, S.H., and Shi, Y. (2014). Three-dimensional structure of human γ -secretase. *Nature* *512*, 166–170.
- Lyumkis, D., Brilot, A.F., Theobald, D.L., and Grigorieff, N. (2013). Likelihood-based classification of cryo-EM images using FREALIGN. *J. Struct. Biol.* *183*, 377–388.
- Mao, Y., Wang, L., Gu, C., Herschhorn, A., Désormeaux, A., Finzi, A., Xiang, S.H., and Sodroski, J.G. (2013). Molecular architecture of the uncleaved HIV-1 envelope glycoprotein trimer. *Proc. Natl. Acad. Sci. USA* *110*, 12438–12443.
- McMullan, G., Chen, S., Henderson, R., and Faruqi, A.R. (2009a). Detective quantum efficiency of electron area detectors in electron microscopy. *Ultramicroscopy* *109*, 1126–1143.
- McMullan, G., Clark, A.T., Turchetta, R., and Faruqi, A.R. (2009b). Enhanced imaging in low dose electron microscopy using electron counting. *Ultramicroscopy* *109*, 1411–1416.
- McMullan, G., Faruqi, A.R., Henderson, R., Guerrini, N., Turchetta, R., Jacobs, A., and van Hoften, G. (2009c). Experimental observation of the improvement in MTF from backthinning a CMOS direct electron detector. *Ultramicroscopy* *109*, 1144–1147.
- McMullan, G., Faruqi, A.R., Clare, D., and Henderson, R. (2014). Comparison of optimal performance at 300keV of three direct electron detectors for use in low dose electron microscopy. *Ultramicroscopy* *147*, 156–163.
- Meyer, R.R., Kirkland, A.I., Dunin-Borkowski, R.E., and Hutchison, J.L. (2000). Experimental characterisation of CCD cameras for HREM at 300 kV. *Ultramicroscopy* *85*, 9–13.
- Meyerson, J.R., Kumar, J., Chittori, S., Rao, P., Pierson, J., Bartesaghi, A., Mayer, M.L., and Subramaniam, S. (2014). Structural mechanism of glutamate receptor activation and desensitization. *Nature* *514*, 328–334.
- Mooney, P. (2007). Optimization of image collection for cellular electron microscopy. *Methods Cell Biol.* *79*, 661–719.
- Ruskin, R.S., Yu, Z., and Grigorieff, N. (2013). Quantitative characterization of electron detectors for transmission electron microscopy. *J. Struct. Biol.* *184*, 385–393.

- Scheres, S.H. (2010). Classification of structural heterogeneity by maximum-likelihood methods. *Methods Enzymol.* *482*, 295–320.
- Scheres, S.H. (2012). RELION: implementation of a Bayesian approach to cryo-EM structure determination. *J. Struct. Biol.* *180*, 519–530.
- Scheres, S.H. (2014). Beam-induced motion correction for sub-megadalton cryo-EM particles. *eLife* *3*, e03665.
- Scheres, S.H., Gao, H., Valle, M., Herman, G.T., Eggermont, P.P., Frank, J., and Carazo, J.M. (2007). Disentangling conformational states of macromolecules in 3D-EM through likelihood optimization. *Nat. Methods* *4*, 27–29.
- Seidelt, B., Innis, C.A., Wilson, D.N., Gartmann, M., Armache, J.P., Villa, E., Trabuco, L.G., Becker, T., Mielke, T., Schulten, K., et al. (2009). Structural insight into nascent polypeptide chain-mediated translational stalling. *Science* *326*, 1412–1415.
- Shi, Y. (2014). A glimpse of structural biology through X-ray crystallography. *Cell* *159*, 995–1014.
- Sigworth, F.J. (1998). A maximum-likelihood approach to single-particle image refinement. *J. Struct. Biol.* *122*, 328–339.
- Sigworth, F.J., Doerschuk, P.C., Carazo, J.M., and Scheres, S.H. (2010). An introduction to maximum-likelihood methods in cryo-EM. *Methods Enzymol.* *482*, 263–294.
- Song, F., Chen, P., Sun, D., Wang, M., Dong, L., Liang, D., Xu, R.M., Zhu, P., and Li, G. (2014). Cryo-EM study of the chromatin fiber reveals a double helix twisted by tetranucleosomal units. *Science* *344*, 376–380.
- Stark, H., Zemlin, F., and Boettcher, C. (1996). Electron radiation damage to protein crystals of bacteriorhodopsin at different temperatures. *Ultramicroscopy* *63*, 75–79.
- Suloway, C., Pulokas, J., Fellmann, D., Cheng, A., Guerra, F., Quispe, J., Stagg, S., Potter, C.S., and Carragher, B. (2005). Automated molecular microscopy: the new Legimon system. *J. Struct. Biol.* *151*, 41–60.
- Taylor, K.A., and Glaeser, R.M. (1974). Electron diffraction of frozen, hydrated protein crystals. *Science* *186*, 1036–1037.
- Trabuco, L.G., Villa, E., Schreiner, E., Harrison, C.B., and Schulten, K. (2009). Molecular dynamics flexible fitting: a practical guide to combine cryo-electron microscopy and X-ray crystallography. *Methods* *49*, 174–180.
- Typke, D., Downing, K.H., and Glaeser, R.M. (2004). Electron microscopy of biological macromolecules: bridging the gap between what physics allows and what we currently can get. *Microsc. Microanal.* *10*, 21–27.
- Urban, K.W. (2011). Electron microscopy: The challenges of graphene. *Nat. Mater.* *10*, 165–166.
- Vinothkumar, K.R., Zhu, J., and Hirst, J. (2014). Architecture of mammalian respiratory complex I. *Nature* *515*, 80–84.
- Wolf, M., Garcea, R.L., Grigorieff, N., and Harrison, S.C. (2010). Subunit interactions in bovine papillomavirus. *Proc. Natl. Acad. Sci. USA* *107*, 6298–6303.
- Yan, Z., Bai, X.C., Yan, C., Wu, J., Li, Z., Xie, T., Peng, W., Yin, C.C., Li, X., Scheres, S.H., et al. (2015). Structure of the rabbit ryanodine receptor RyR1 at near-atomic resolution. *Nature* *517*, 50–55.
- Yu, X., Jin, L., and Zhou, Z.H. (2008). 3.88 Å structure of cytoplasmic polyhedrosis virus by cryo-electron microscopy. *Nature* *453*, 415–419.
- Yu, X., Ge, P., Jiang, J., Atanasov, I., and Zhou, Z.H. (2011). Atomic model of CPV reveals the mechanism used by this single-shelled virus to economically carry out functions conserved in multishelled reoviruses. *Structure* *19*, 652–661.
- Zalk, R., Clarke, O.B., des Georges, A., Grassucci, R.A., Reiken, S., Mancina, F., Hendrickson, W.A., Frank, J., and Marks, A.R. (2015). Structure of a mammalian ryanodine receptor. *Nature* *517*, 44–49.
- Zhang, X., Settembre, E., Xu, C., Dormitzer, P.R., Bellamy, R., Harrison, S.C., and Grigorieff, N. (2008). Near-atomic resolution using electron cryomicroscopy and single-particle reconstruction. *Proc. Natl. Acad. Sci. USA* *105*, 1867–1872.
- Zhang, X., Jin, L., Fang, Q., Hui, W.H., and Zhou, Z.H. (2010). 3.3 Å cryo-EM structure of a nonenveloped virus reveals a priming mechanism for cell entry. *Cell* *141*, 472–482.
- Zhao, G., Perilla, J.R., Yufenyuy, E.L., Meng, X., Chen, B., Ning, J., Ahn, J., Gronenborn, A.M., Schulten, K., Aiken, C., and Zhang, P. (2013). Mature HIV-1 capsid structure by cryo-electron microscopy and all-atom molecular dynamics. *Nature* *497*, 643–646.
- Zhou, Z.H., and Chiu, W. (1993). Prospects for using an IVEM with a FEG for imaging macromolecules towards atomic resolution. *Ultramicroscopy* *49*, 407–416.
- Zhou, Z.H., Dougherty, M., Jakana, J., He, J., Rixon, F.J., and Chiu, W. (2000). Seeing the herpesvirus capsid at 8.5 Å. *Science* *288*, 877–880.